2013 European Control Conference (ECC)
July 17-19, 2013, Zürich, Switzerland.

A high-fidelity simulation model for an asymmetric nonlinear electrothermal actuator

Leonardo Angelo Muffato* and Dominique-Stephan Kunz*

Abstract— **In this paper a high-fidelity single-input and single-output (SISO) simulation model for an asymmetric nonlinear electrothermal actuator is presented. The model was mainly developed using grey-box system identification and considers energy conversion and energy flow between electrical, thermal and mechanical domains. It is particularly useful for investigation of different control strategies (control performance, control stability, actuator life cycle and energy consumption) for plants employing SAUTER AXT211 thermal actuator. Some insights are given in the process of system identification, model optimization and validation using measured data. Correlation between simulation results and measured data is investigated, as well as simulation model confidence.**

I. INTRODUCTION

Electrothermal actuators convert energy from electrical domain into thermal domain, and from thermal domain into mechanical domain (motion) [1]. Electrothermal actuators are employed in automotive, aerospace and industrial applications [2] as well for the heating, ventilation, and air-conditioning (HVAC) sector. In [3], a model of thermo regulated valves is proposed for performing simulations of the control of fancoils with thermal actuators and a SAUTER RSK 401 unit.

SAUTER AG develops, produces and markets electrothermal actuators for usage in HVAC sector, specially for room temperature control. SAUTER has recently developed a new generation of actuator, named AXT211, and with this new development there was also the need for creating a simulation model for investigating different issues like:

- actuator performance under different environment temperatures T_U, $T_U \in [0, \cdots, 50\,^{\circ}\mathrm{C}]$
- actuator performance under different supply voltages U, $U \in [19, \cdots, 29\ \mathrm{VAC/VDC}]$
- appropriate control strategies for this actuator, capable of dealing with an asymmetric behaviour due to different opening and closing times. Asymmetry origins due to different heat transfer rates during actuator opening ($P_{PTC} = 1$) and during closing ($P_{PTC} = 0$), heat balance is written in (16).
- maximizing control performance and stability
- maximizing actuator lifetime
- minimizing energy consumption

Dynamics from room temperature control are usually very slow, with time constants in the order of 15 hours and higher. This makes it very time-consuming, to experiment different control adjustments in real time. Using simulation for investigating control adjustment with different combination of plants (for example the combination of thermal actuator with different valves, heat exchangers and room types) is specially interesting since one can save a lot of time. Computation of system dynamics using numerical simulation is performed in a fraction of time of real process duration. For example, the simulation of a room temperature control system during a whole year using recorded weather data for a given location with a higher-order simulation model (using CARNOT blockset [4]) may be performed in less than 2 hours with a standard personal computer (PC).

*Fr. Sauter AG. Im Surinam 55, 4016 Basle-Switzerland. Website: http://www.sauter-controls.com Email:leonardo.muffato, dominique.kunz@ch.sauter-bc.com

II. DEFINITIONS

Let $\mathbb{R}, \mathbb{R}^m, \mathbb{R}^{m\times n}, \mathbb{N}$ denote the field of real numbers, the set of column real vectors of length m, the set of m by n real matrices, the set of non-negative integers. The L^p-norm for a vector $z \in \mathbb{R}^m$, may be written [5]:

$$\|z\|_p := \left(\sum_{v=1}^{m} |z_v|^p\right)^{1/p} \tag{1}$$

and for a matrix $Z \in \mathbb{R}^{m\times n}$:

$$\|Z\|_p := \left(\sum_{v=1}^{m}\sum_{w=1}^{n} |Z_{vw}|^p\right)^{1/p} \tag{2}$$

(1) and (2) are for $p = 2$ respectively the euclidian and Frobenius norm.

III. GREY-BOX SYSTEM IDENTIFICATION

The principle of this heuristic identification method is to combine two sources of information that are available during model development: a prior knowledge of the system dynamics, and response data from experiments. A brief introduction to this method will be given in this section, the interested reader may find more information in [6]. Furthermore, acc. to the definitions of [6], identification of physically based model is called white-box identification. What actually turns it into grey-box identification, as presented in this work, is the incorporation of (black-box) polynomial models (14) and (21), as well as the empirical step for considering ($\delta W = 0$) as presented in section VI-B.

Consider the multiple-input, multiple-output (MIMO) dynamic system:

$$\dot{x} = f(x, u, d) \tag{3}$$

$$y = g(x, u, d) \tag{4}$$

with $u \in \mathbb{R}^m$ inputs to the system, $x \in \mathbb{R}^n$ system states, $y \in \mathbb{R}^k$ system outputs, $d \in \mathbb{R}^q$ disturbances to the system. A simulation model is created using prior knowledge of the system dynamics:

$$\dot{x}_m = f_m(x_m, u, d, p) \tag{5}$$

$$y_m = g_m(x_m, u, d, p) \tag{6}$$

with $x_m \in \mathbb{R}^{n_m}$ model states, $y_m \in \mathbb{R}^k$ model outputs, $p \in \mathbb{R}^r$ a vector of unknown simulation model parameters. A number N of experiments with the real system are performed, and u_i, d_i, y_i are recorded, $i = 1, \cdots, N$. Notice that a notation is used here, for which z_i is not the ith component of the z vector, but a matrix with measured data at ith experiment. Thus, $u_i \in \mathbb{R}^{ci \times m}$, $d_i \in \mathbb{R}^{ci \times q}$ and $y_i \in \mathbb{R}^{ci \times k}$, with $ci \in \mathbb{N}$ the number of samples acquired at ith experiment. Now, finding out p may be formulated as a mathematical optimization problem. We define an appropriate cost function, for the least squares method it is:

$$J(p) = \sum_{i=1}^{N} \|y_i - y_m(u_i, d_i, p)\|_2^2 \tag{7}$$

and the nonlinear constrained optimization (solutions for this kind of problem are proposed in [7],[8] and [9]):

$$\begin{aligned} &\min_p \ J(p) \\ &\text{s.t. } p \in P \subset \mathbb{R}^r \end{aligned} \tag{8}$$

In the case of unconstrained optimization ($P = \mathbb{R}^r$), also called nonlinear regression, it is possible to use the Gauß-Newton Method for finding p as described in [10]. An implementation of this method was used to improve simulation models of train brake system components, as presented in [11]. Different than the Newton Method and other optimization methods, Gauß-Newton has the advantage that it does not calculate the Hessian of $J(p)$, thus reducing computing time.

A. Calculation of derivatives

A decisive step for a successful grey-box system identification is the computation of Jacobian and Hessian matrices. [12] proposes using finite differences, [13] proposes algorithmic differentiation (AD). In this work we decided to use finite differences, since this method is directly supported by the optimization functions from Optimization Toolbox™ 5.0 (The MathWorks Inc.).

One issue was observed during identification / optimization of different sub-models and test cases during this work: when using a variable step size (differential equation) explicit solver for evaluating (7), it took more iterations for the optimization of (8) to converge, and solution converged to a local minimum p_1 with cost function $J(p_1)$. The same identification / optimization when performed using a fixed step size explicit solver, took less iterations to converge, and solution converged to a better local minimum (maybe a global minimum) p_2, with $J(p_2) < J(p_1)$. An explanation for this deviations may be found looking at (10). Acc. to [12], using a first-order Taylor expansion, the directional derivative of the function $j(z)$ at a point z_0 is simply identified with the difference between two of its values:

$$grad(z_0)_i = \frac{\partial j(z_0)}{\partial z_i} \approx \frac{j(z_0 + \varepsilon e_i) - j(z_0)}{\varepsilon} \tag{9}$$

with $i = 1, \cdots, r$, ε a conveniently chosen small parameter (to avoid linearization and round-off errors) and $(e_i)_{i=1,\cdots,r}$ denotes the canonical basis of $\mathbb{R}^r$. Since $j(z)$ is evaluated numerically, there is an error $\phi(z)$ associated to it. (9) may be rewritten:

$$\frac{\partial j(z_0)}{\partial z_i} \approx \frac{\tilde{j}(z_0 + \varepsilon e_i) + \phi(z_0 + \varepsilon e_i) - (\tilde{j}(z_0) + \phi(z_0))}{\varepsilon} \tag{10}$$

with $\tilde{j}(z)$ the exact (ideal) solution. The error propagated to the calculation of derivatives is:

$$\epsilon_d = \frac{\phi(z_0 + \varepsilon e_i) - \phi(z_0)}{\varepsilon} \tag{11}$$

Although this issue was not investigated in detail during this work, it is expected that $\epsilon_d \approx 0$ for fixed step solvers and $\epsilon_d > 0$ for variable step size solvers, since the latter ones adjust step size depending on: the value of z, the relative and the absolute tolerances. $\epsilon_d > 0$ induces an error in the calculation of (9) at each iteration, which leads the optimization problem as stated in (8) to change p in a direction different than the optimum direction. As a result, optimization takes more iterations to converge and convergence is less precise than when using fixed step size solvers.

Finally, in order to keep errors as small as possible, derivatives calculation using finite differences was performed by using a fixed step size solver.

IV. Test rig

Measurements performed for simulation model development used following hardware: Thermal actuator: SAUTER AXT211, attached to a valve type VUL015F310. Linear displacement was measured using an inductive displacement sensor (LVDT series) from the company Micro-Epsilon. Measurements were performed in a climate control chamber, KB53 series from the company Binder. Data acquisition was performed using an UEIDaq Power DAQ PD2-MF-64-333/16H, temperature measurements were performed with thermocouples and FLUKE Hydra Series II data acquisition unit. Data acquisition control was performed using an automation station EY-AS525 [14], from the company SAUTER as well as the Data Acquisition Toolbox™.

Simulations and optimization were performed using a commercial software package (MATLAB® 7.1, Simulink® 7.5, Optimization Toolbox™ 5.0, Data Acquisition Toolbox™ 2.13, The MathWorks Inc.).

V. Electrothermal actuator AXT211

AXT211 [15], [16], is the new generation of SAUTER electrothermal actuators, which operates silently, requires no maintenance, is water-proof with IP54 and fits a wide number of valves from different manufacturers thanks to a patented facility which automatically compensates for the closing

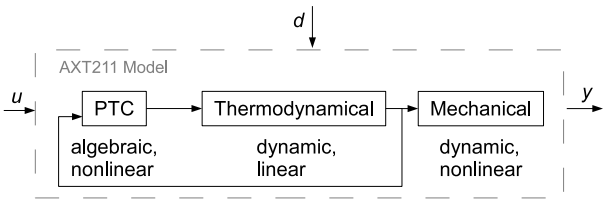

Fig. 1. AXT211 model and its submodels

TABLE I
VARIABLES USED IN AXT211 MODEL

Variables	Description	Unit
u	normalized control input	$[0, \ldots, 1]$
k_U	Supply Voltage	V
P_{PTC}	PTC power consumption	W
R_{PTC}	PTC electrical resistance	Ω
T_G	Actuator housing temperature	°C
T_P	Wax cartridge temperature	°C
T_U	Actuator environment temperature	°C
x_P	Wax cartridge stroke	mm
x_V	Valve stroke	mm

dimension. It has an electrically heated PTC element, an overload-protected wax expansion cartridge that transfers its stroke directly to the attached valve. When the supply voltage is switched on, the PTC heats the wax cartridge, which after achieving a temperature of about 60 °C begins displacing the valve rod for a stroke of 4.5 mm, which is achieved after ca. 5 minutes of power on at environment temperature of 25 °C. When switched off, the wax element transfers heat to the actuator environment by natural convection, cools down and the valve is closed by means of a spring.

VI. AXT211 MODEL

The AXT211 model is a nonlinear, time-invariant continuous dynamical system which may be represented by an explicit state-space model:

$$\dot{x} = f(x, u, d) \tag{12}$$

$$y = g(x) \tag{13}$$

where $x = [T_P, T_G, x_P]^T \in \mathbb{R}^3$ is the state vector, $u \in \mathbb{R}_{[0,1]}$ is the normalized control input, $d = [k_U, T_U]^T \in \mathbb{R}^2$ the disturbance vector, $y = [P_{PTC}, R_{PTC}, T_P, T_G, x_P, x_V]^T \in \mathbb{R}^6$ the output vector, which gathers the main physical quantities. For a description of variables see Table I. The model also has a parameter vector $p \in \mathbb{R}^{22}$, with parameters found using system identification, which will be described in the next subsections. For grey-box system identification, the AXT211 model was divided into submodels comprehending different physical domains: PTC, thermodynamical and mechanical domain.

A. PTC model

The electrical resistance of the PTC thermistor used in AXT211 was calculated from measurements of voltage and current, and increases with temperature [17] in a nonlinear manner. The approximation of this characteristic was investigated with exponential functions as well as with polynomials different orders, although the best approach to test data in a least-squares sense was found using a polynomial 5^{th} order, as seen in Fig. 2.

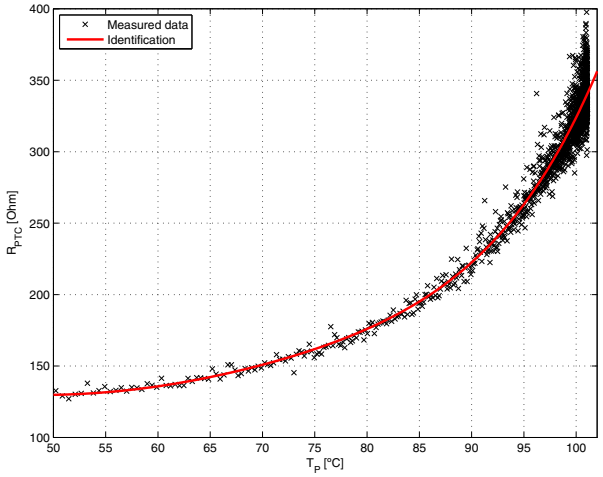

Fig. 2. Modelling PTC Resistance

The PTC model was validated for $T_P \in [30, \cdots, 101\,°\text{C}]$ and may be written:

$$R_{PTC} = a_n T_P^n + a_{n-1} T_P^{n-1} + \cdots + a_1 T_P + a_0 \tag{14}$$

with $a_n \neq 0$. Finally, the PTC element power consumption is:

$$P_{PTC} = \frac{(k_U * u)^2}{R_{PTC}} \tag{15}$$

B. Thermodynamical model

Investigations were performed with a first-order thermodynamical model, but simulation results were not very accurate compared with measured data. A second-order model was investigated, and results fitted much better. The latter model will be described in this section.

The thermodynamical model represents temperature dynamics from wax cartridge. Wax cartridge temperature may be modelled using the first law of thermodynamics ($\mathrm{d}U = \delta Q - \delta W$):

$$\frac{\mathrm{d}\,(m_P c T_P)}{\mathrm{d}t} = P_{PTC} - \lambda_{PG}(T_P - T_G) - \delta W \tag{16}$$

with λ_{PG} thermal conductance from wax cartridge to actuator housing, δW the work perfomed by wax cartridge expansion. In (16) it was assumed, that electrical power consumed by PTC element is converted to thermal energy without losses. Modelling of δW using x_P and valve force characteristics $F(x_P)$ did not lead to good simulation results compared to measured data. Since force acting between valve and actuator could not be measured, and due to the fact that there is a lack of information on wax cartridge thermal expansion process, i.e., the behaviour of thermal expansion coefficient at different temperatures is unknown,

an attempt was made to identify the thermodynamical model considering ($\delta W = 0$). (16) is rewritten:

$$\dot{T}_P = \frac{P_{PTC} - \lambda_{PG}(T_P - T_G)}{C_P} \tag{17}$$

with $C_P = m_P c$ the thermal capacity from wax cartridge. Since the parameters C_P and λ_{PG} are identified from measured data, the influence of missing δW in (17) is compensated as far as possible. Simulation results confirm a very good fidelity to measured data, as presented in section VII. Temperature dynamics from actuator housing are written:

$$\dot{T}_G = \frac{\lambda_{PG}(T_P - T_G) - \lambda_{GU}(T_G - T_U)}{C_G} \tag{18}$$

with C_G the thermal capacity from actuator housing, λ_{GU} thermal conductance from actuator housing to environment.

C. Mechanical model

The mechanical model represents dynamics of AXT211 wax cartridge stroke x_P and valve stroke x_V. It is a first order model with nonlinear gain characteristics:

$$\dot{x}_P(t) = \frac{k_P(x_P)(T_P - T_{P,x_P=0}) - x_P(t)}{\tau_P} \tag{19}$$

and backlash, which is formulated based on [18]:

$$x_V(t) = \begin{cases} x_P(t) + c & \text{if } x_P(t) < x_V(t - \mathrm{d}t) - c \\ x_P(t) - c & \text{if } x_P(t) > x_V(t - \mathrm{d}t) + c \\ x_V(t - \mathrm{d}t) & \text{otherwise} \end{cases} \tag{20}$$

where c is half of the deadband width, t is time. where k_P is a nonlinear gain function, $k_P : \mathbb{R}^{\geq 0} \rightarrow \mathbb{R}^{>0}$, $T_{P,x_P=0}$ is the wax cartridge temperature at which piston displacement begins, τ_P a time constant for dynamics of mechanical model.

For investigating gain characteristics at different wax cartridge temperatures, a temperature control loop was implemented. Set point was a temperature step function, with values changing at every thirty minutes in a 2 °C step. Thirty minutes for a 2 °C step is a long time, but this was necessary in order that a stationary state of x_V was achieved. Measurements were performed inside a climate chamber, which maintained constant environment temperature to minimize disturbances in temperature value over time.

Results from closed loop measurements may be observed in fig. 3. For $T_P = 60\,^{\circ}\mathrm{C}$, a very small gain is observed, and for $T_P = 68\,^{\circ}\mathrm{C}$, gain achieves its maximum value. k_P may be approximated from measured data as a quadratic function:

$$k_P(x_P) = a x_P^2 + b x_P + c, \quad with \quad a < 0. \tag{21}$$

Looking at fig. 3, it is also possible to identify actuator backlash. When the temperature step function is going up from 52 °C to 70 °C, different stationary values are observed than when temperature is decreasing ($t > 330 min.$). Backlash was considered within simulation using formulation shown in (20). Comparison of mechanical model with real actuator behaviour may be seen in fig. 4.

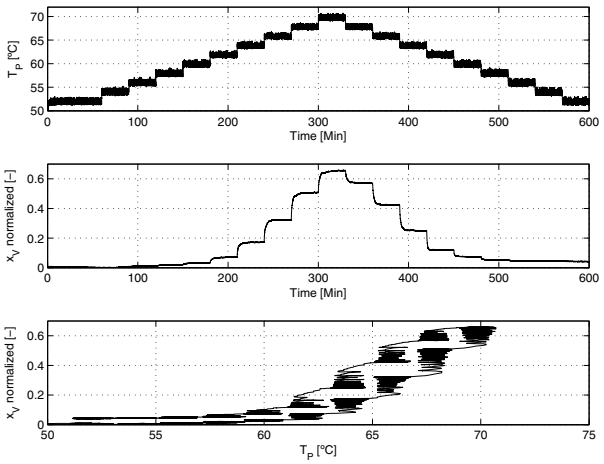

Fig. 3. Measured data for gain and backlash investigation

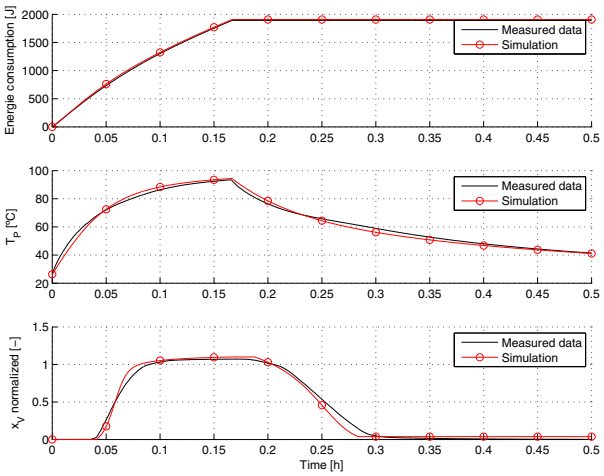

Fig. 5. Validation AXT211 model, Test case 1

Notice that for identifying mechanical model parameters using (8), backlash as formulated in (20) must be temporarily disabled in the simulation model, since this function is not differentiable.

VII. Validation with test data

For model identification and validation, 54 different test cases were defined and hundreds of hours of measured data were compared to simulation data. Fig. 4 to 7 shows comparison for 3 different test cases. Validation was performed in 3 steps: 1) Choose of appropriate test case according to the submodel being validated (not all test cases are suitable for all submodels). 2) The submodel is simulated using the same inputs from measurements. 3) Simulation results are compared to measurement data. The simulation model was mainly validated using test cases also used for identification. The mean value for accuracy with all suitable test cases ($\bar{\xi}$) is 0.93, 0.95 and 0.84 for the PTC, thermodynamical and mechanical model respectively.

The correlation between simulation results and measured data (simulation model accuracy) ξ is calculated using the

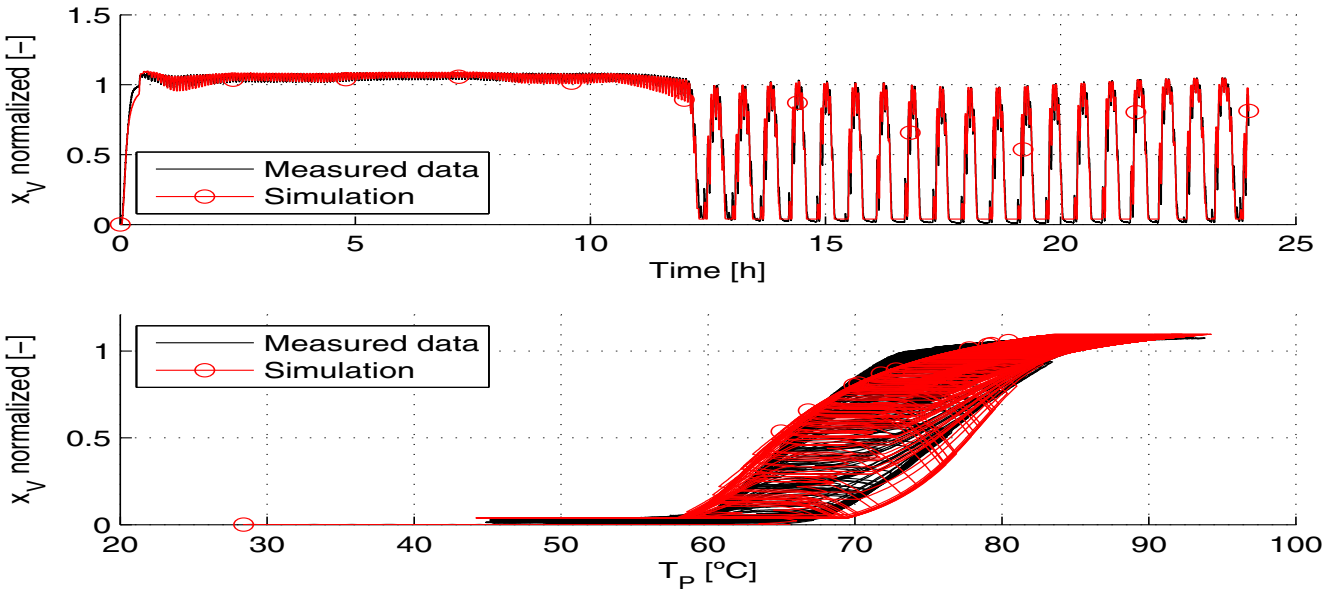

Fig. 4. Validation mechanical model

TABLE II
SUBMODEL ACCURACY (ξ) WITH DIFFERENT TEST CASES

Test case	PTC	Thermodynamical	Mechanical
1	0.9528	0.9781	0.9083
2	0.9582	0.9781	0.9355
3	0.9598	0.9711	0.9216

L^2-norm (euclidian norm):

$$\xi = 1 - \frac{\|y_m - y\|_2}{\|y\|_2} \tag{22}$$

$\xi = 1$ means 100% model accuracy and could only be achieved if we had the perfect plant model. Table II shows ξ for chosen test cases, calculated using P_{PTC} for PTC model, T_P for thermodynamical model, x_v for mechanical model and measured k_U and d as input to simulation model. All values presented in Table II are higher than 0.90, which means simulation results are at least 90% accurate with measured data. Outputs from thermodynamical model are even better with $\xi > 0.97$ for test cases 1 to 3. Model accuracy is considered good, in view of the difficulties existing in modelling of electrothermal actuators and the lower order of the simulation model. For the development of a simulation model which achieves higher values for ξ, it might be necessary to increase model order, model complexity and to perform separate measurements and identification of individual electrothermal actuator components.

VIII. AXT211 SIMULATION MODEL CONFIDENCE

Thermal actuators are known to have a high standard deviation, originated mainly from wax cartridge manufacture procedure. This issue was investigated measuring x_v of a sample with fifteen AXT211 thermal actuators same model

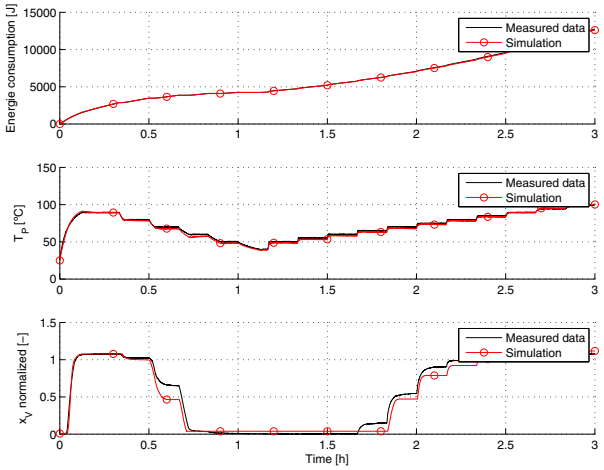

Fig. 6. Validation AXT211 model, Test case 2

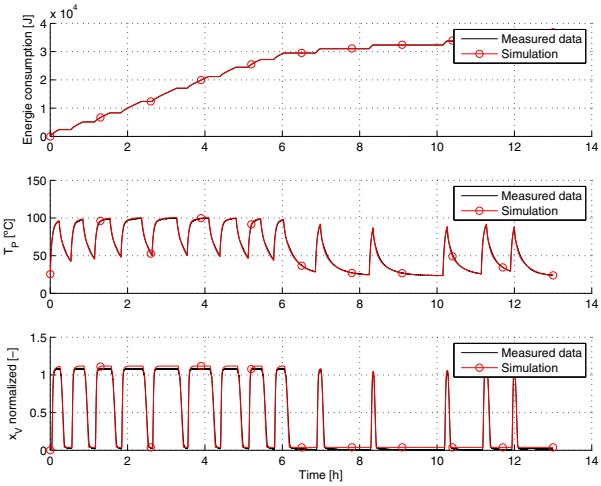

Fig. 7. Validation AXT211 model, Test case 3

produced at three different manufacturing dates. Measurements were performed in a climate chamber with constant environment temperature. Actuators were subjected to four different input signals, some of them using pulse-width modulation (PWM):

$$u(t) = \begin{cases} \text{step from } 0 \text{ to } 1 & \text{for } t \leq 1 \\ \text{PWM with } f_{PWM} \text{ high} & \text{for } 1 < t \leq 3 \\ \text{PWM with } f_{PWM} \text{ medium} & \text{for } 3 < t \leq 4.5 \\ \text{PWM with } f_{PWM} \text{ low} & \text{for } t > 4.5 \end{cases}$$

with t measurement time in hours, $\eta_{PWM} = 50\%$ duty cycle and f_{PWM} frequency.

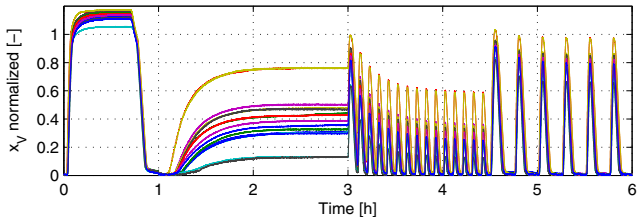

Fig. 8. AXT211 spread investigation

Measurement results are presented in fig. 8. High variations from mean value are observed specially for controlling AXT211 with PWM at high and at medium frequency. It is not recommended to control AXT211 at these frequencies, since actuators behave differently for same input signal. Controllers should operate AXT211 at f_{PWM} low, also called on-off operation. Detailed information for controlling AXT211 is given in [19].

The confidence interval P may be calculated:

$$P = \left[\bar{x}_v - t\frac{\sigma}{\sqrt{n}}, \bar{x}_v + t\frac{\sigma}{\sqrt{n}}\right] \tag{23}$$

with $\bar{x}_v$ the sample mean value, $n = 15$ the sample size, $t_{(\gamma=99\%)} = 2.98$ as in [20], σ the standard error. P for AXT211 may be graphically visualized as the grey region in fig. 9. The results obtained with the simulation model are also displayed, and it can be seen that $x_{v,Simulation}$ is always inside or very close to P, attesting for simulation model confidence with real actuator behaviour.

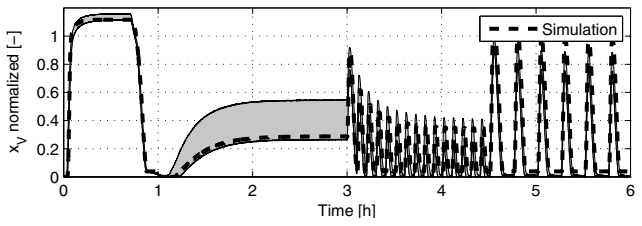

Fig. 9. AXT211 confidence interval (grey region) for $n = 15, \gamma = 99\%$

IX. Conclusion

In this paper a novel simulation model for an asymmetric nonlinear electrothermal actuator was presented. Although there were many unknown parameters housed in different physical domains, it was possible to create a high-fidelity model(this is attested by validation with 54 different test cases) employing system identification and optimization methods. The correlation between simulation results and measured data is higher than 90%, as presented in section VII. Simulation model confidence was investigated by comparing simulation results with measured data of fifteen AXT211 thermal actuators of same model but from different production series. Simulation results are always inside or very close to confidence interval, as exploited in section VIII. The model is simple to implement (in a PC with an available ODE solver) and has only three states, what leads to affordable computation time.

Further investigation could be a model sensitivity analysis, to investigate influence of some design variables over actuator performance (for example thermal conductivity and capacity of actuator housing, gain from PTC element, etc.).

References

[1] J. L. Pons, *Emerging Actuator Technologies: A Micromechatronic Approach*. John Wiley & Sons, 2005.

[2] (2012) VERNET SA. [Online]. Available: http://www.vernet.fr

[3] dr.ir. P.J. Lute, "Control of fancoils by thermo regulated valves. simulations, control system tests, measurements of air flow patterns, noise measurements. rapport nr. k-205," Technische Universiteit Delft, Tech. Rep., 1994.

[4] *CARNOT Blockset - Conventional And Renewable Energy Systems Optimization Blockset - User's Guide*, Version 1.0 ed., Solar-Institut Juelich und Scientific Computers GmbH, 1999.

[5] K. Koenigsberger, *Analysis 2*. Springer, 2004.

[6] T. P. Bohlin, *Practical Grey-box Process Identification: Theory and Applications (Advances in Industrial Control)*. Springer, 2006.

[7] M. Papageorgiou, *Optimierung. Statische, dynamische, stochastische Verfahren fuer die Anwendung*. Oldenbourg, 1991.

[8] M. Ulbrich and S. Ulbrich, *Nichtlineare Optimierung*. Birkhaeuser, 2012.

[9] M. Sobotka, "Skriptum zur vorlesung optimierungsverfahren in der automatisierungstechnik," Lehrstuhl fuer Steuerungs- und Regelungstechnik der Technische Universitaet Muenchen, 07 2009.

[10] W. Dahmen and A. Reusken, *Numerik fuer Ingenieure und Naturwissenschaftler*. Springer, 2008.

[11] L. A. Muffato, "Definitions for the c-pressure simulation of a pneumatic brake systems for rail vehicles and their performance components," Technische Universitaet Muenchen and KNORR-BREMSE Systeme fuer Schienenfahrzeuge GmbH," Term paper, 2009.

[12] E. Laporte and P. Tallec, *Numerical methods in sensitivity analysis and shape optimization*. Birkhaeuser, 2003.

[13] M. Diehl, "Script for numerical optimization course, b-kul-h03e3a," Optimization in Engineering Center (OPTEC) and ESAT-SCD, K.U. Leuven, Tech. Rep., 2009.

[14] *modu525: Modular automation station with BACnet/IP and web server. Product Data Sheet, PDS 92.016*, SAUTER AG. [Online]. Available: http://www.sauter-controls.com

[15] *AXT201, 211: Thermal actuator for unit valves, with stroke indicator. Product Data Sheet, PDS 55.100*, SAUTER AG. [Online]. Available: http://www.sauter-controls.com

[16] *New thermal actuator. Product information, e/Doc. No.: D100043336*, SAUTER AG, 2010.

[17] B. J. B. Whitman and J. Tomczyck, *Refrigeration and Air Conditioning Technology*. Delmar Cengage Learning, 2004.

[18] G. Tao and P. V. Kokotovic, *Adaptive Control of Systems with Actuator and Sensor Nonlinearities*. John Wiley & Sons, 1996.

[19] *SAUTER AXT211, Regelungsrichtlinien. Handbuch 7010082001A*, SAUTER AG, 2011.

[20] L. Papula, *Mathematische Formelsammlung fr Ingenieure und Naturwissenschaftler*. Vieweg, 2006.